Influence of using innovative turbulators on the exergy and energy efficacy of flat plate solar collector with DWCNTs-TiO_2/water nanofluid

Yacine Khetib [a,b], Ali Alzaed [c], Ahamd Tahmasebi [d], Mohsen Sharifpur [e,f,*], Goshtasp Cheraghian [g,*]

[a] Mechanical Engineering Department, Faculty of Engineering, King Abdulaziz University, Jeddah 80204, Saudi Arabia
[b] Center Excellence of Renewable Energy and Power, King Abdulaziz University, Jeddah 80204, Saudi Arabia
[c] Architectural Engineering Department, Faculty of Engineering, Taif University, Taif, Saudi Arabia
[d] Independent Researcher
[e] Department of Mechanical and Aeronautical Engineering, University of Pretoria, Pretoria 0002, South Africa
[f] Department of Medical Research, China Medical University Hospital, China Medical University, Taichung, Taiwan
[g] Technische Universität Braunschweig, 38106 Braunschweig, Germany

A R T I C L E I N F O

Keywords:
FPSC
Innovative turbulator
Hybrid nanofluid
Exergy and energy efficacies
Two-phase flow

A B S T R A C T

This study investigates the effect of using turbulators with innovative geometrie (TIG) and DWCNTs-TiO_2/water hybrid nanofluid (HNF) on thermal–hydraulic performance, exergy and energy efficacies of flat plate solar collector (FPSC) using a mixed two-phase model (TPM). Finite volume technique (FVT), SIMLPLEC algorithm and FLUENT software are used. The numerical study is performed for nano-additives concentrations (ϕ) of 1 to 3%, Reynolds numbers (Re) from 7000 to 28000, and PR of 1, 2, 3, and 4 of the proposed TIG in turbulent flow regime. The results show that the average Nusselt number (Nu_{ave}) increases by augmenting the Re and ϕ. In addition, at Re = 28,000 and ϕ = 3%, the installation of TIG with PR = 4 within the solar collector (SC) increases the Nu_{ave} by 63.46%. In the case of ϕ = 3% and by augmenting the Re from 7000 to 28000, energy and exergy efficacies increase by 22.19% and 23.26% for PR = 4 and PR = 1, respectively.

Introduction

Solar energy is one of the most popular types of energy for human use these days. Meanwhile, the equipment for exploiting this energy is of particular interest to researchers [1–6]. One of the most extensively used equipment is solar collectors, and researchers are thinking of improving their efficiency in various ways every day [7–12]. One way to increase the efficiency of solar collectors is to focus on improving heat transfer in them. In the meantime, augmenting the heat transfer rate (HTR) using passive methods has always been the focus of researchers [13–15]. One of these approaches is to use turbulators with dissimilar shapes to enhance HTR [16–19]. The use of nanomaterials has also been highly considered by researchers in recent decades [20–27]. Afshari et al. [28] considered the influence of turbulator on thermal performance (η) inside the SC, experimentally and numerically. Based on the results obtained from their study, the experimental and numerical findings were in good agreement with high accuracy. Also, the use of a turbulator increases the efficacy of the SC by 72.41%.

Rostami et al. [3] considered the influence of elliptical tubes on the exergy efficacy of water-multi-walled carbon nanotubes in a FPSC using FVT and FLUENT software. According to their results, the maximum augmentation in the efficacy of the FPSC is 17.11% when elliptical tubes are used.

Sakhaei and Valipour [29] experimentally inspected the effect of height and roughness on a parabolic solar collector (PSC). According to their results, the use of roughness and augmenting its length intensifies the η of the PSC. Also, the η increases by augmenting the roughness height. In addition, the maximum augmentation in η of the SC was 97.6%.

Hosseini et al. [30] experimentally examined the effect of rotary turbulators with twisted tape to increase HTR in the solar desalination system. According to their results, the use of a rotary tubulator with twisted tape can improve the output efficacy to its maximum value. Besides, in the solar desalination system, the maximum output efficacy was 87.11% lower than the solar desalination system with a rotary turbulator.

Ibrahim et al. [31] numerically measured the effect of TIG on the

* Corresponding authors at: Department of Mechanical and Aeronautical Engineering, University of Pretoria, Pretoria 0002, South Africa (M. Sharifpur).
E-mail addresses: mohsen.sharifpur@up.ac.za (M. Sharifpur), g.cheraghian@tu-braunschweig.de (G. Cheraghian).

Nomenclature

Symbols

c_P	Specific heat, (J/kgK)
D_h	Hydraulic diameter, (m)
f	Friction factor
k	Thermal conductivity, (W/mK)
P	Pressure, (Pa)
T	Temperature (K)
V	Velocity

Greek symbols

μ	Dynamic viscosity (mPa.s)
ρ	Density (m^3/kg)
η	efficiency

Subscriptions

np	Nanoparticle
nf	Nanofluid

Abbreviations

FVT	finite volume technique
PEC	thermal–hydraulic performance
η_{en}	energy efficiency
η_{ex}	exergy efficiency
PR	pitch ratios
SC	solar collector
FPSC	flat plate solar collector
HNF	hybrid nanofluid

exergy efficacy of a HNF in a SC. In this study, they employed a hybrid water/aluminum oxide-multi-walled carbon nanotube nanofluid using the FVT. Their results revealed that exergy efficacy decreases with the height and twisted ratio of turbulators.

Yan et al. [32] numerically considered the influence of using U-shaped PSC tubes filled with non-Newtonian two-phase hybrid nanofluids (TPHNFs) using the FVT and FLUENT software. They used a surface-to-surface model to model radiation energy and employed a mixed TPM to model a two-phase non-Newtonian HNF. Based on their findings, the use of U-shaped absorber tubes increases the η of the PSC by 45.11%.

Shahsavar Goldanlou et al. [33] considered the impact of using HNF on the flow field and HTR within a PSC FVT and the k-ω model to examine the flow field. Their results indicated that the HTR intensifies with augmenting the nano-additive concentration. Also, the maximum augmentation in η of the PSC was 46.89% using HNFs more than case of water-based fluid.

Waghole et al. [34] investigated the influence of employing twisted tape on the thermal and hydraulic performance of water-silver nanofluid in a linear PSC. Their results showed that augmenting the ϕ of silver nanoparticles and Re results in a substantial increase in the η of the linear PSC. In addition, augmenting the pitch of the twisted tape increases the HTR and ΔP.

Nazir et al. [35] numerically inspected the influence of water/aluminum oxide nanofluid on energy efficacy and exergy of a linear PSC for Re from 500 to 1500 and volume fractions of 1 to 4%. Their results demonstrated that amplifying the Re and ϕ increases energy and exergy efficacy.

The impact of using porous obstacles on the fluid flow and HTR of nanofluid inside the PSC was experimentally examined by Reddy et al. [36]. They found that augmenting the porosity of the obstacles augments the η of the PSC. However, augmenting the porosity increases the ΔP. Also, the η of the PSC with porous obstacles increases by 57.34% compared to the SC without porous obstacles.

Ma et al. [37] numerically investigated the influence of using hot tubs on the free convection of Cu/EG-water nanofluid in the space between adiabatic cylinders for Rayleigh numbers of 10^3 to 10^5 and ϕ from zero to 0.05. They reported that the Nu_{ave} enhances significantly with the Rayleigh number. Also, the use of nanofluids has shown much higher η than water-based fluid and ethylene glycol.

Reddy et al. [38] numerically inspected the influence of porous obstacles on the flow field and HTR of water-aluminum oxide nanofluid in a turbulent flow regime inside a PSC using k-ε turbulence model. They reported that porous obstacles and nanofluid increase the η of the SC. Also, the maximum augmentation in HTR when porous obstacles were employed was 18.45%.

The impact of twisted tape on the fluid flow and HTR within a PSC using computational fluid dynamics was numerically inspected by Jaramillo et al. [39]. Their numerical results revealed that augmenting the Re and the pitch ratio in the twisted tape increases the η of the SC. Also, the maximum intensification in η was 19% when the twisted tape was employed.

Zhu et al. [40] used FVT and the k-ω turbulence model for evaluating the effect of corrugated tapes in a PSC. Based on their findings, the maximum intensification in η of the SC at Re = 20,000 was 156.51%.

Dezfulizadeh et al. [41]numerically studied the influence of a hybrid TIG on the exergy efficacy of a triple HNF in a heat exchanger exposed to a magnetic field. Their study was carried out for Re from 4000 to 16,000 and volume fractions of zero to 3%. Their findings indicated that the installation of a hybrid turbulator rises the exergy efficacy in the heat exchanger. Also, the use of hybrid turbulators in the counterclockwise direction is more suitable in terms of exergy efficacy.

In this study, a special type of turbulator with new geometries has been used. This turbulator has been studied in several of PR values. Simultaneous investigation of energy and exergy efficienciess and PEC value is of other features of this study. Also in this study, polymeric hybrid nanofluid has been used, which has been less discussed in previous studies.

According to the researched performed so far, the thermal and hydraulic performance, exergy efficacy, and energy efficacy of DWCNTs-TiO_2/water TPHNF turbulent flow in SCs equipped with innovative turbulators have not been studied. Consequently, in this numerical research, thermal and hydraulic performance of DWCNT- TiO_2/water HNF with $1 \le \phi \le 3\%$, $7000 \le Re \le 28000$, and the PR = 1, 2, 3, and 4 for turbulators is investigated for turbulent flow regime.

Mathematical model and equations

Fig. 1 displays the schematic view of the SC containing TIG. As seen, the absorber tube is a part of the SC. The lengths of absorber tube and TIG are 800 mm and 300 mm, respectively. The TIG is installed in the middle of the absorber tube. The distance of TIG from both sides of the tube is 250 mm. For simulating the radiation, the surface-to-surface model is employed. Furthermore, the k-ε turbulence model and the SIMPLEC algorithm are respectively applied to solve the turbulent flow and discretization of the equations.

Table 1 presents the geometry specification of TIG.

The DWCNTs-TiO_2/water TPHNF is employed as the heat transfer fluid. The thermophysical characteristics of the used materials are reported in Table 2.

For simulating the DWCNT-TiO_2/water HNF flow through the SC, the mixed TPM is implemented. The governing equations of the problem are expressed in Table 3.

In Equation (18) $\dot{Q}_{HTF}$ is calculated from Equation (19). In this equation $T_{i,HTF}$ is the fluid temperature at the inlet of heat exchanger. T_s is the surface temperature of the collector absorber pipe. V_I is also the hybrid nanofluid velocity. Also,η_P is the efficiency of the pump used in the parabolic solar collector cycle and its value is 80%.

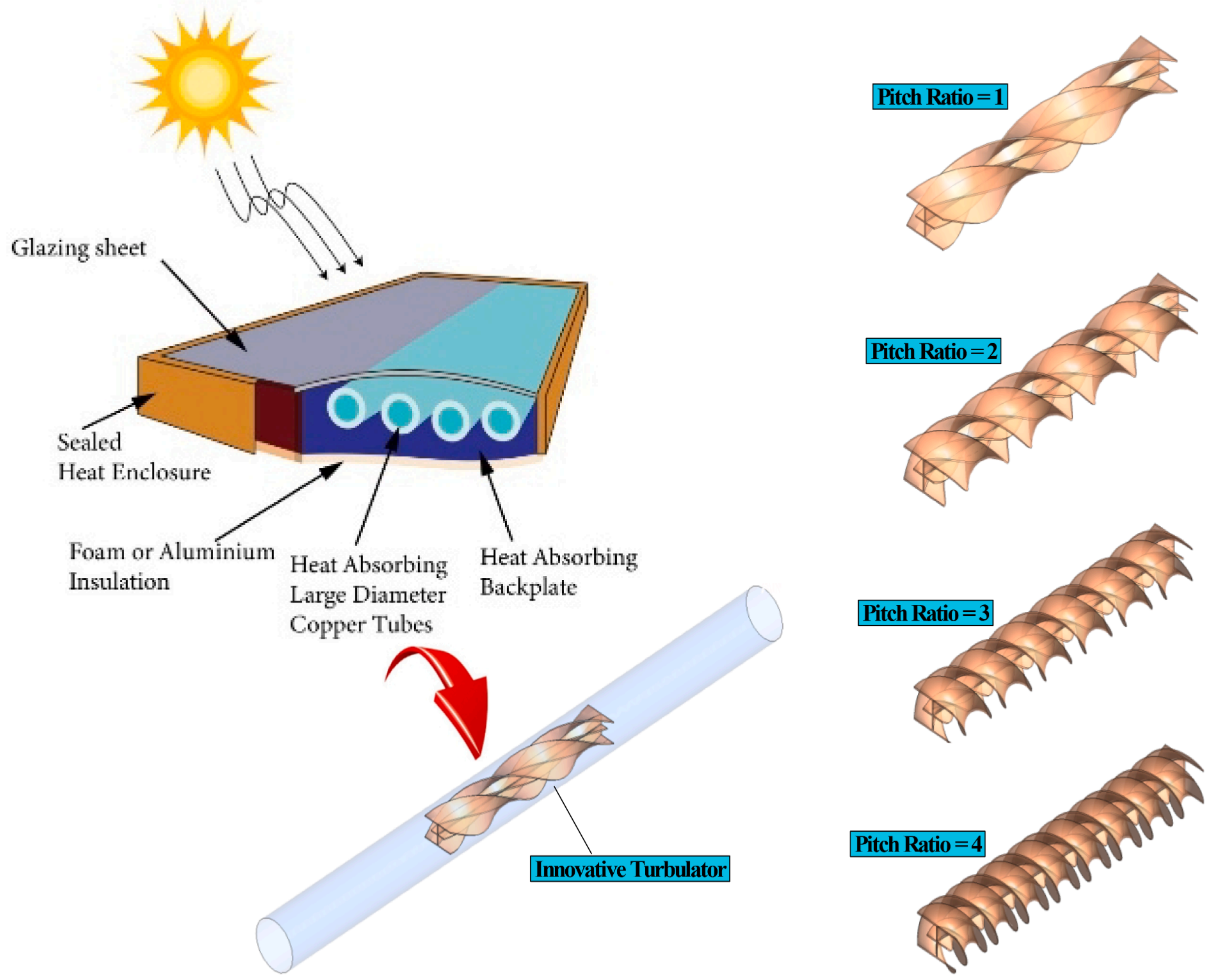

Fig. 1. Schematic of the SC equipped with TIG.

Table 1
Characteristics of the considered TIG.

Dimension	Size
L	300 mm
D	60 mm
PR	1, 2, 3, 4

Table 2
Thermophysical specification of water and nano-additives [42,43].

Property	Water	TiO_2	DWCNT
$\rho(kg.m^{-3})$	998.2	4250	2100
$c_P(J.kg^{-1}.K^{-1})$	4182	686.2	710
$k(W.m^{-1}.K^{-1})$	0.6	80.2	3000
$\mu(kg.m^{-1}.s^{-1})$	0.001003	–	–

Numerical modeling

Past research has shown that using numerical methods to solve complex fluid flow and heat transfer equations can be very useful. In fact, using numerical methods or computational fluid dynamics can reduce the time and cost of performing experiments [49–53]. In the present study, FLUENT software version 18.2 is used for numerical simulations. First, the geometry of the SC is prepared in three dimensions using the design modeler module. In order to discretize the computational area into a number of control volumes, the geometry of the SC is gridded. After performing the grid independence test and ensuring the number of elements in the computational area, the grid geometry is exported into FLUENT software. The problem is solved on the steady assumption and the solver is pressure-based. The DWCNTs-TiO_2/water HNF flow is simulated using a mixed TPM. In order to model the turbulent flow, the standard k-ε turbulence model is used. The boundary conditions at the input of the PSC are $7000 \leq Re \leq 28000$, the $\phi = 1$ to 3% of TiO_2 and DWCNT nanoparticles, and twisted ratios of 1, 2, 3, and 4 of the TIG. The Least Squares Cell-Based model is applied for discretization. The standard model is applied to discretize the pressure, and the power-law model is employed for momentum, turbulent kinetic energy, and volume fraction equations.

Grid independence assessment

In Fig. 2, for grids with different number of points, the Nu_{ave} is calculated to select the best grid in order to make the results independent of the grid. In order to obtain a proper grid that leads to the independence of the findings from the number of grid points, the Nu_{ave} for DWCNTs-TiO2/water HNF inside a SC with a TIG is calculated (Fig. 2). It can be concluded that the grid with 2132044 nodes is appropriate for a SC with a TIG. Further intensification of this grid resolution does not change the values of the Nu_{ave}. Therefore, the grid resolution of 2132044 is selected for the present simulations.

Table 3
Governing equations [44–48].

Equation name	Formula	Eq. No.
continuity equation	$\nabla\left(\rho_m \vec{U}_m\right) = 0$	(1)
mixture velocity or mass-averaged velocity	$\vec{U}_m = \frac{\rho_s \phi_s \vec{U}_s + \rho_{bf}\phi_{bf}\vec{U}_{bf}}{\rho_m}$	(2)
mixture density	$\rho_m = \rho_s\phi_s + \rho_{bf}\phi_{bf}$	(3)
momentum equation	$\rho_m\left(\vec{U}_m \nabla \vec{U}_m\right) = -\nabla \vec{P} + \mu_m\left(\nabla \vec{U}_m + \left(\nabla \vec{U}_m\right)^T\right) + \nabla\left(\rho_{bf}\phi_{bf}\vec{U}_{dr,bf}\vec{U}_{dr,bf} + \rho_s\phi_s\vec{U}_{dr,s}\vec{U}_{dr,s}\right) + \rho_m \vec{g}$	(4)
drift velocity of particles	$\vec{U}_{dr,bf} = \vec{U}_{bf} - \vec{U}_m$	(5)
base fluid drift velocity	$\vec{U}_{dr,s} = \vec{U}_s - \vec{U}_m$	(6)
energy equation	$\nabla\left(\rho_{bf}\phi_{bf}\vec{U}_{bf}h_{bf} + \rho_s\phi_s\vec{U}_s h_s\right) = \nabla\left(\left(\phi_{bf}k_{bf} + \phi_s k_s\right)\nabla \vec{T}\right)$	(7)
volume fraction equation	$\nabla\left(\rho_s\phi_s\vec{U}_m\right) = -\nabla\left(\rho_s\phi_s\vec{U}_{dr,s}\right)$	(8)
slip velocity	$\vec{U}_{bf,s} = \vec{U}_{bf} - \vec{U}_s$	(9)
drift velocity and relative velocity	$\vec{U}_{dr,s} = \vec{U}_{s,bf} - \frac{\rho_s\phi_s}{\rho_m}\vec{U}_{bf,s}$	(10)
velocity is through the Schiller and Naumann	$\vec{U}_{bf,s} = \frac{d_p^2}{18\mu_{bf} f_d}\frac{\rho_s - \rho_m}{\rho_s}\vec{\alpha}$	(11)
	$f_d = 1 + 0.15\mathrm{Re}_s^{0.687}$	
	$\vec{\alpha} = \vec{g} - \left(\vec{U}_m \nabla \vec{U}_m\right)$	
Reynolds number	$\mathrm{Re}_s = \frac{\vec{U}_m d_p \rho_m}{\mu_m}$	(12)
describe the k-ε model	$\nabla\left(\rho_m\vec{U}_m k\right) = \nabla\left[\left(\mu_m + \frac{\mu_{t,m}}{\sigma_k}\right)\nabla k\right] + G_{k,m} - \rho_m\varepsilon$	(13)
	$\nabla\left(\rho_m\vec{U}_m \varepsilon\right) = \nabla\left[\left(\mu_m + \frac{\mu_{t,m}}{\sigma_\varepsilon}\right)\nabla \varepsilon\right] + \frac{\varepsilon}{k}\left(c_1 G_{k,m} - c_2\rho_m\varepsilon\right)$	
turbulent viscosity	$\mu_{t,m} = C_\mu \rho_m \frac{k^2}{\varepsilon}$	(14)
production rate	$G_{k,m} = \mu_{t,m}\left(\nabla \vec{U}_m + \left(\nabla \vec{U}_m\right)^T\right)$	(15)
Thermal energy	$\eta_c = \frac{E_c}{I \bullet A} = \frac{Q_{in} \bullet \rho_{in} \bullet c_{p,in} \bullet (T_{out} - T_{in})}{6 \bullet 10^4 \bullet \mathrm{I} \bullet \mathrm{A}}$	(16)
efficacy	$\eta_n = \frac{E_n}{I \bullet A} = \frac{p_{fo} \bullet Q_{in} \bullet \rho_{in} \bullet c_{p,in} \bullet \left(\mathrm{T}_{\mathrm{fo,out}} - \mathrm{T}_{\mathrm{in}}\right) + (1 - \mathrm{p}_{\mathrm{fo}})\mathrm{Q}_{\mathrm{in}} \bullet \rho_{\mathrm{in}} \bullet \mathrm{c}_{\mathrm{p,in}} \bullet \left(\mathrm{T}_{\mathrm{fi,out}} - \mathrm{T}_{\mathrm{in}}\right)}{6 \bullet 10^4 \bullet \mathrm{I} \bullet \mathrm{A}}$	(17)
Exergy efficacy	$\eta_{ex} = \frac{\dot{Q}_{HTF} - \dot{m}_{HTF}c_{p,HTF}\ln\left(\frac{T_\infty}{T_{i,HTF}}\right)}{-\dot{Q}_{HTF} - \dot{m}_{CF}c_{p,CF}\ln\left(\frac{T_{o,CF}}{T_{i,CF}}\right) + V_I\eta_P}$	(18)
Heat transfer rate	$\dot{Q}_{HTF} = h(T_{i,HTF} - T_s)$	(19)

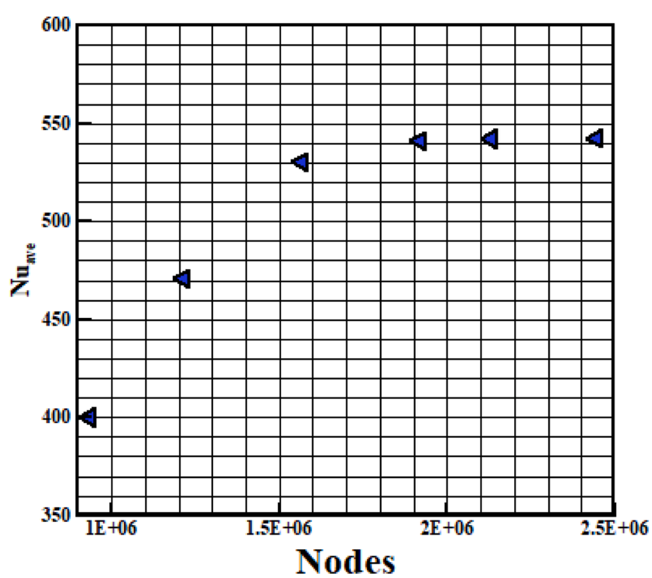

Fig. 2. Nu_{ave} for DWCNTs-TiO_2/water hybrid nanofluid in SC containing a TIG for Re = 28000, ϕ = 3%, PR = 4, and different grid resolutions.

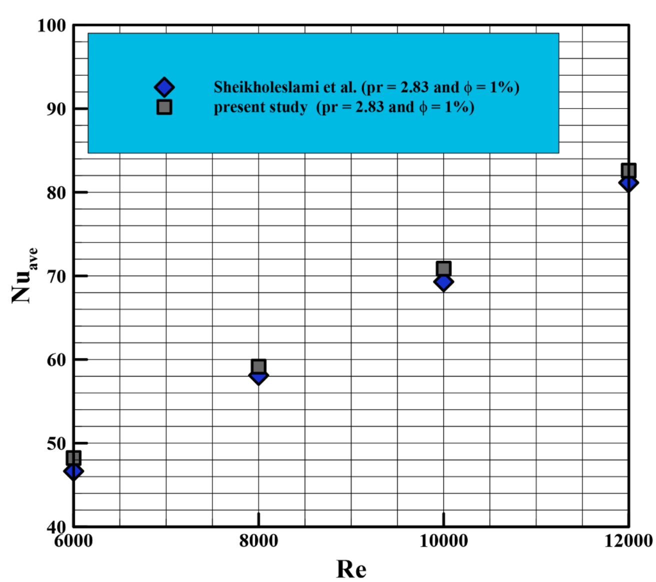

Fig. 3. Nu_{ave} versus Re: comparison between the results obtained from the present simulations and the ones reported by Sheikholeslami et al. [54].

Verification

The numerical findings is verified according to the similar model presented by Sheikholeslami et al. [54] and the Nu_{ave} are compared (Fig. 3). As observed, the difference between the amounts of the Nu_{ave} gained in the present solutions is minor (about 3.11%) compared to the

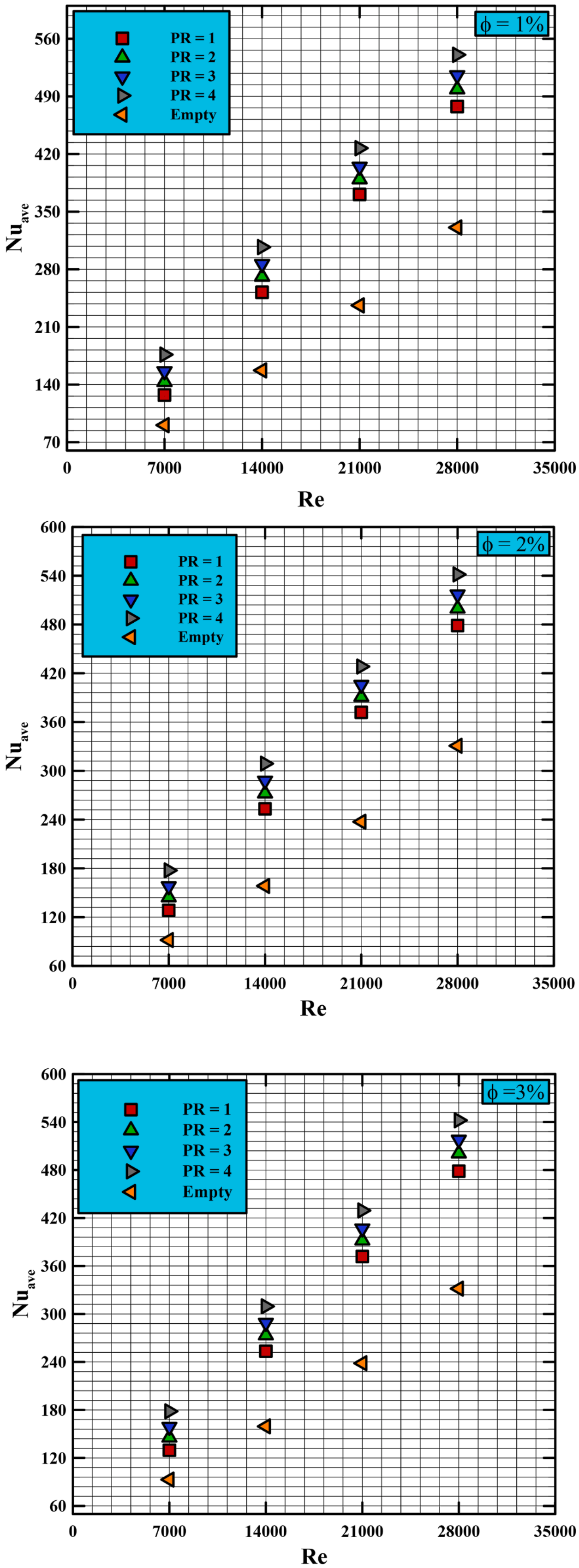

Fig. 4. Nu_{ave} versus Re in a SC containing a TIG with various twisted ratios for different nano-additives concentrations.

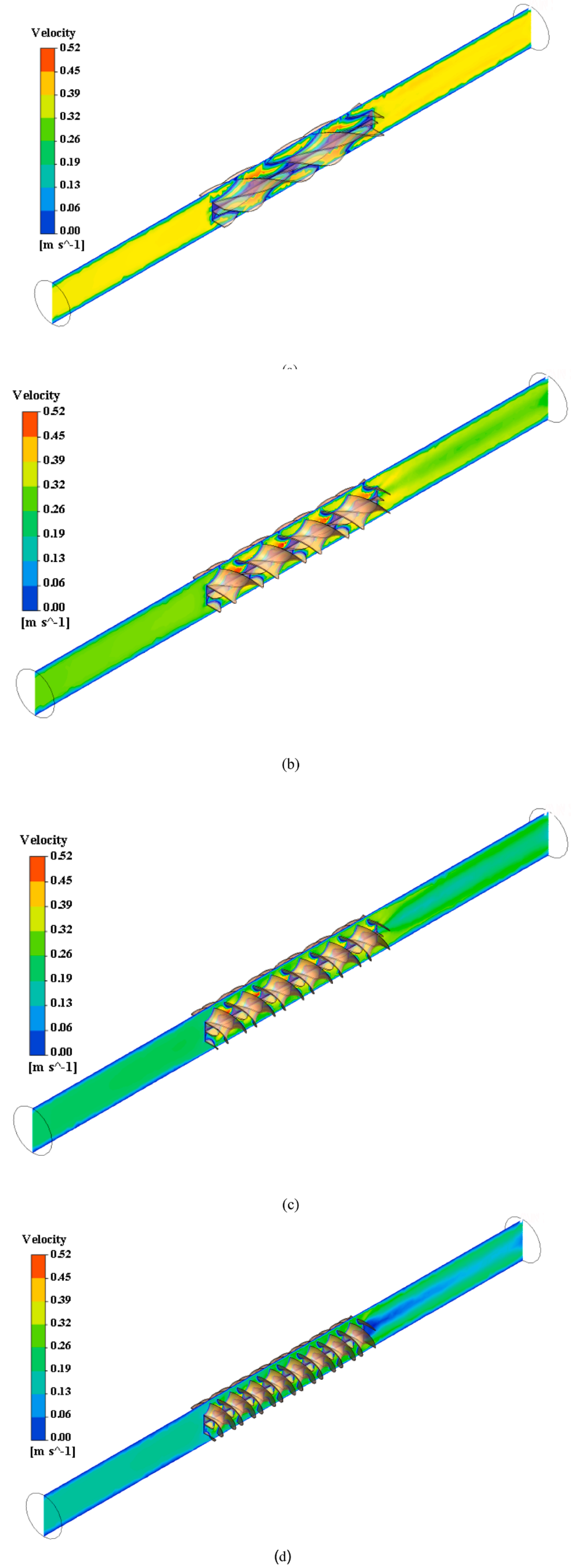

Fig. 5. Contours of velocity for TPHNFs for $\phi = 3\%$, Re = 28000, and (a) PR = 1, (b) PR = 2, (c) PR = 3, and (d) PR = 4.

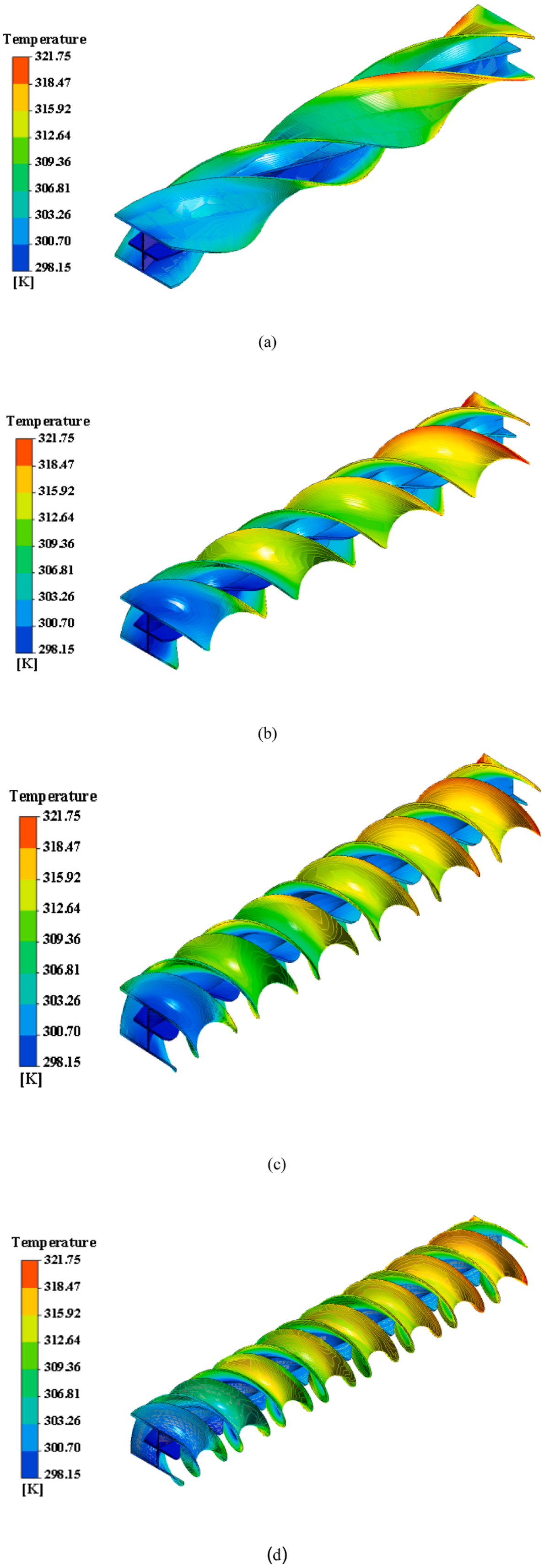

Fig. 6. Temperature contours for TPHNFs for ϕ = 3%, Re = 28000, and (a) PR = 1, (b) PR = 2, (c) PR = 3, and (d) PR = 4.

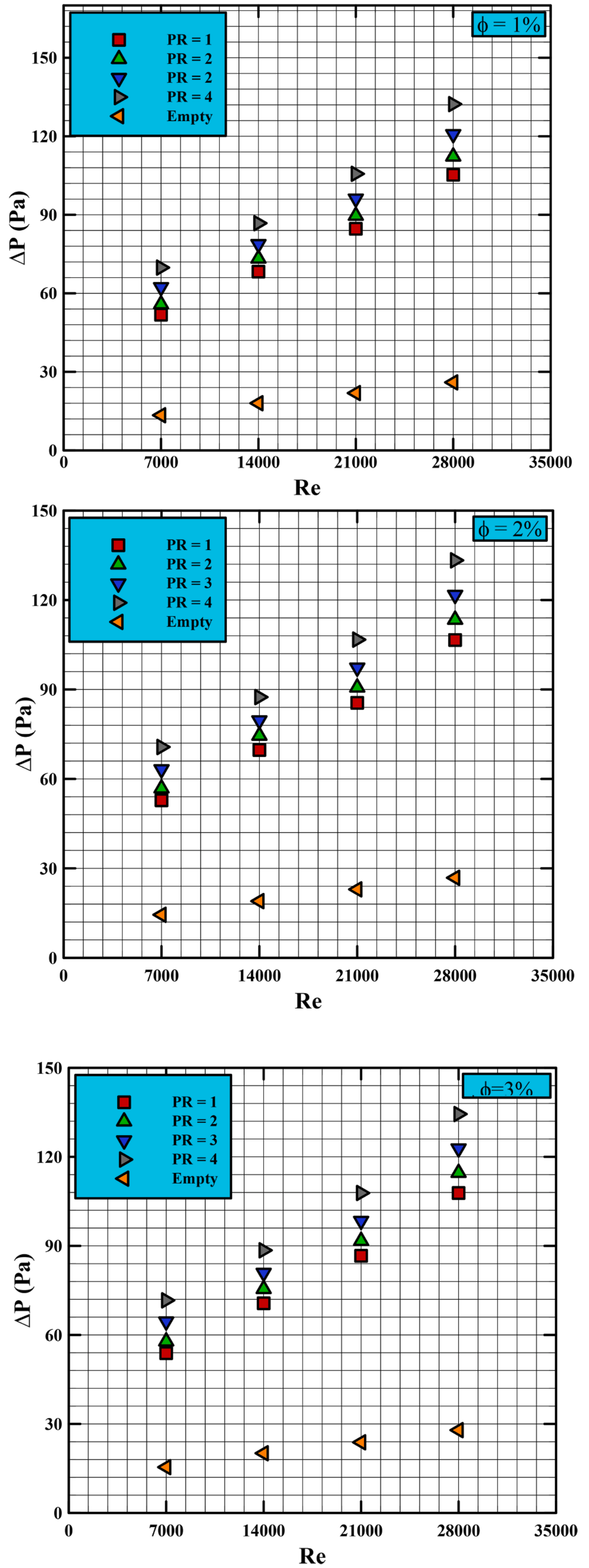

Fig. 7. ΔP against Re in a SC containing a TIG with various PRs for ϕ = 1%, 2% and 3%

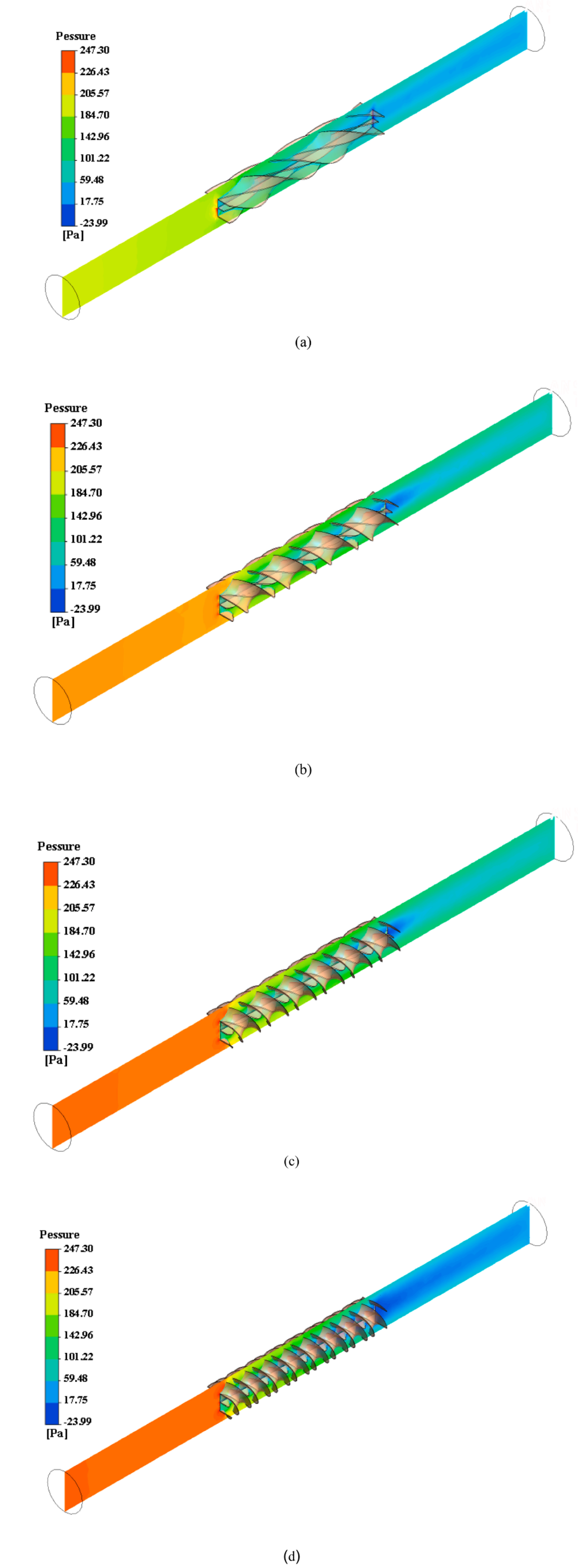

Fig. 8. Pressure-related contours for TPHNFs at $\phi = 3\%$ and Re = 28000 within the SC at (a) PR = 1, (b) PR = 2, (c) PR = 3, and (d) PR = 4.

results of Sheikholeslami et al. [54]. Therefore, the accuracy of the simulations is ensured.

Results and discussion

The findings of simulation are presented in the following. The effect of dissimilar twisted ratios of the TIG inside the SC on the Nu_{ave}, ΔP, thermal–hydraulic evaluation index, and energy efficacy are examined. Moreover, the counters related to velocity, streamlines, pressure, and temperature inside the SC consisting of the TIG with twisted ratios of 1, 2, 3, and 4 are provided for the volume fraction of 3% and Re = 28000.

Effect of TIG twisted ratio on average Nusselt number

Fig. 4 shows the variations of the Nu_{ave} in terms of Re in a SC containing the TIG for various twisted ratios and nano-additives concentrations. As seen, the Nu_{ave} enhances with the Re. In fact, the flow velocity augments by augmenting the Re and consequently, the heat transfer coefficient intensifies, leading to intensification in the Nu_{ave}. At a constant Re, augmenting the turbulent twisted ratio intensifies the mean Nusselt number [33]. Placing the TIG in the SC increases the mixing and turbulence of the DWCNTs-TiO_2/water HNF flow, resulting in an enhancement in the η of the SC. At Re = 28,000, the installation of TIG with PR = 4 increases the Nu_{ave} by 61.23%, 62.87% and 63.46% for $\phi = 1\%$, 2% and 3%, respectively.

In general, with increasing PR value, turbulence and fluctuations in nanofluid flow would be enhanced and heat exchange increases. As a result, the average value of Nusselt number increases [33].

Velocity contours for TPHNF are shown in Fig. 5 for Re = 28000, $\phi =$ 3%, and various PRs. As observed, neighboring the walls, the fluid velocity is equal to the wall velocity because of the no-slip boundary condition. Therefore, the velocity near the wall is zero and increases to touches its highest value at the collector center. According to the velocity contours, it can be observed that the density of streamlines intensifies by augmenting the TIG twisted ratio, leading to amplification in the velocity [33]. As fluid flow hits the TIGs, a separation phenomenon arises; which leads to the creation and rotation of vortices, and consequently η is improved.

Fig. 6 demonstrates the contours of temperature for the TPHNF for ϕ = 3%, Re = 28000, and various PRs.. As seen, the surface temperature of the TIG increases with the collision of the nanofluid flow and the effect of radiation from sunlight.

Effect of innovative turbolator twisted ratio on pressure drop number

Fig. 7 shows the ΔP against Re in a SC containing a TIG with various twisted ratios of 1, 2, 3, and 4. As seen, the ΔP is always increased for all cases by augmenting the Re and TIG twisted ratio. In addition, the ΔP increases with the nano-additive concentration. At Re = 28000, adding the TIG with PR = 4 increases the ΔP by 309.40%, 311.21% and 314.77% for casese of $\phi = 1\%$, 2% and 3%, respectively [33].

The contours of pressure for the TPHNF at Re = 28000 and $\phi = 3\%$ are shown in Fig. 8 for different twisted ratios of 1, 2, 3, and 4. As seen, the streamlines concentration intensifies with augmenting the twisted ratio, leading to an enhancement of the pressure. In addition, the fluid flows between the turbolator blades, causing streamlines to contract. Moreover, with increasing the length of the SC, the pressure reduces. In all cases of turbolator inside the SC, the inlet pressure has its highest amount. The cause for the high pressure in these areas is the flow stagnation because of its hit with the turbolators. Hence, the velocity alters to pressure and then the pressure gradually decreases as the flow passes through the TIG blades.

In general, with increasing PR value, the flow becomes more distorted and turbulent. On the other hand, with increasing PR, the contact surface of the fluid with the TIG wall increases and the amount of shear stress would be more. With increment shear stress, the pressure drop

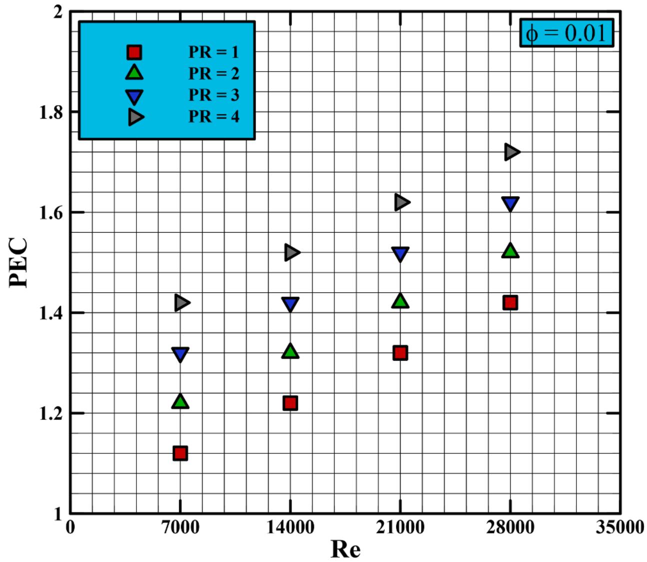

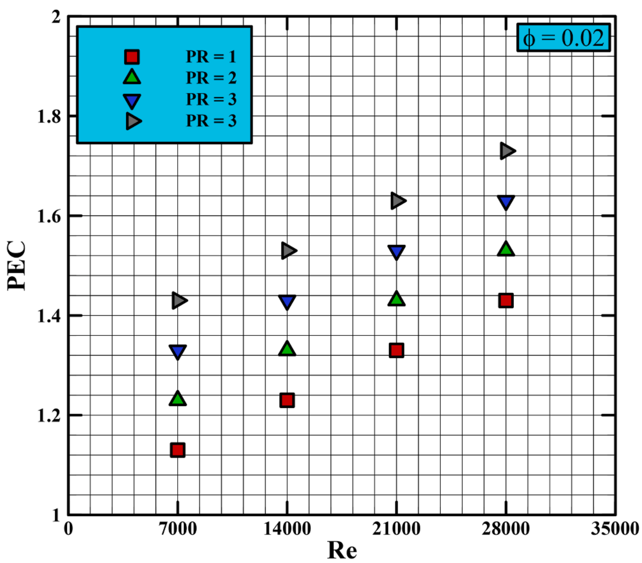

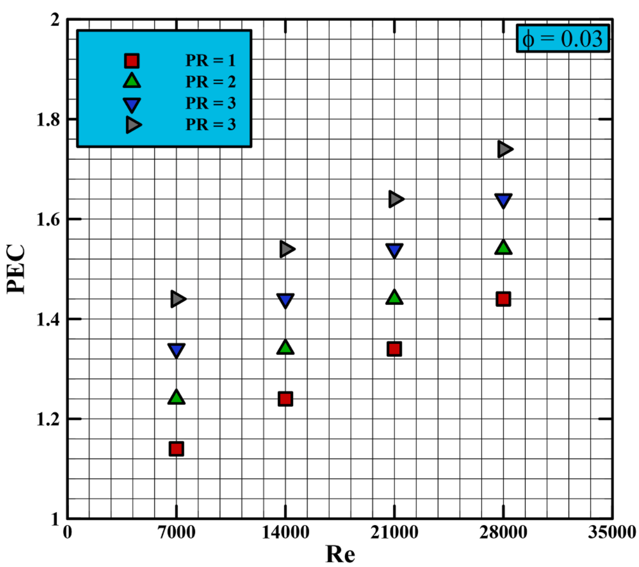

Fig. 9. Thermal hydraulic performance against Re for a SC containing a TIG with various twisted ratios and different nano-additives concentrations.

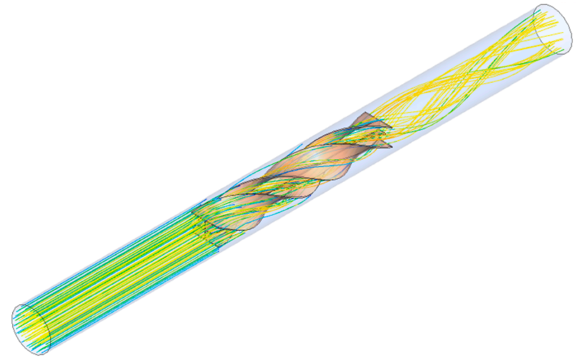

(a)

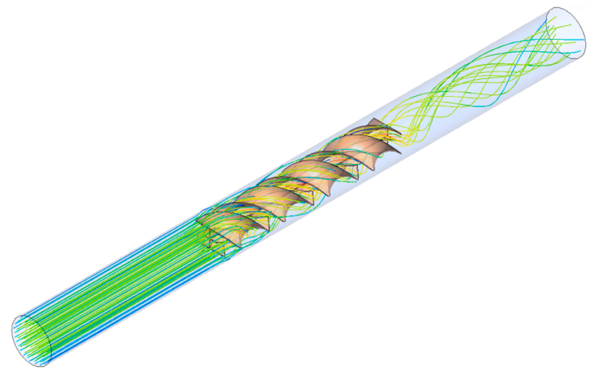

(b)

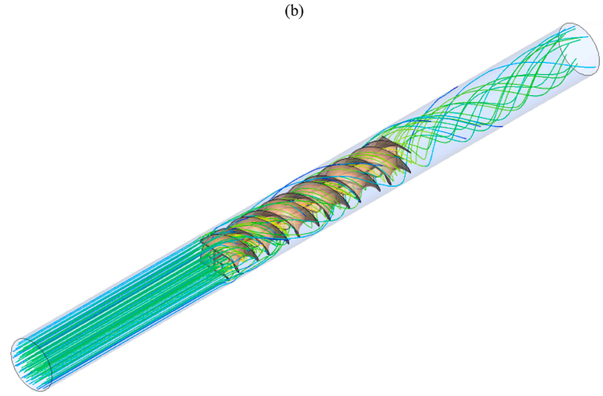

(c)

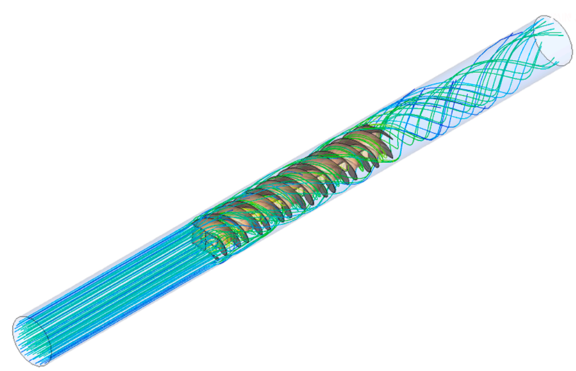

(d)

Fig. 10. Streamline contours for TPHNFs at Re = 28000 and ϕ = 3% at (a) PR = 1, (b) PR = 2, (c) PR = 3, and (d) PR = 4.

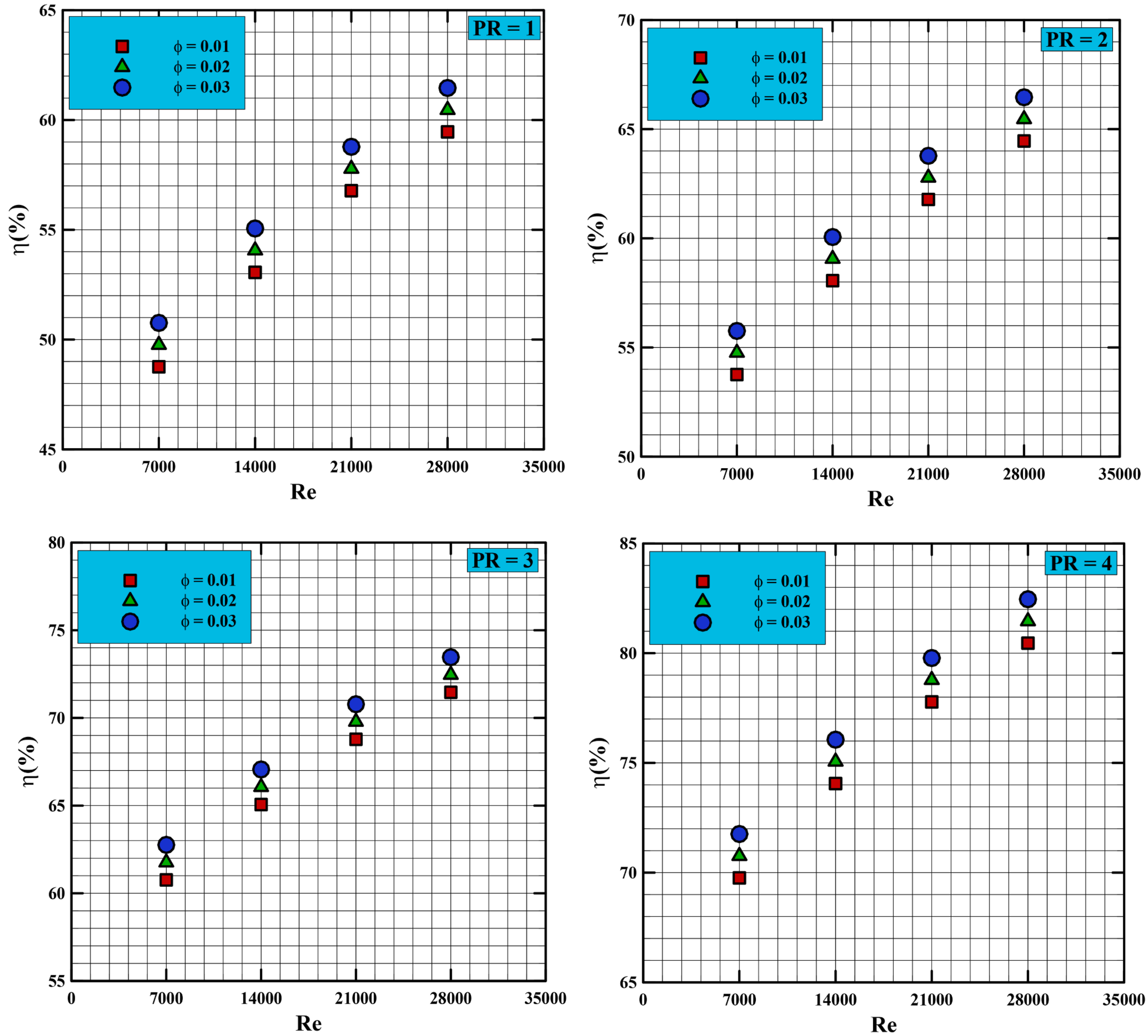

Fig. 11. Energy efficacy against Re in a SC containing a TIG with different twisted ratios and volume fractions.

increases [33].

Effect of TIG twisted ratio on thermal and hydraulic performance coefficient

Changes in thermal–hydraulic coefficient versus Re in a SC containing a TIG with various twisted ratios are shown in Fig. 9 for different twisted ratios of 1, 2, 3, and 4. As seen, in all cases the value of the thermal–hydraulic performance coefficient is more than 1. Thus, it can be understood that installation of a TIG and augmenting its twisted ratio is desirable to enhance thermal–hydraulic index.

Streamline contours for TPHNFs are displayed in Fig. 10 for a $\phi = 3\%$ and $Re = 18000$ within the SC at different PRs. They have been given. As observed, the streamlines concentration intensifies with augmenting twisted ratio in the illuminated TIG.

Effect of TIG twisted ratio on energy efficacy

Energy efficacies against Re in a SC containing a TIG with different twisted ratios and volume fractions are illustrated in Fig. 11. As seen, for all twisted ratios, the energy efficacy is always increased with augmenting Re and nano-additive concentration. Also, the maximum energy efficacy at all Re and volume fractions is related to the state in which the $PR = 4$ is used. At $\phi = 3\%$, by augmenting the Re from 7000 to 28000, the amount of energy efficacy increases by 21.08%, 21.47%, 21.81 and 22.19% for cases of TIGs with $PR = 1$, 2, 3 and 4, respectively [41].

Effect of TIG twisted ratio on exergy efficacy

Exergy efficacy against Re in a SC containing a TIG are shown in Fig. 12 for dissimilar volume fractions and twisted ratios. As seen, the exergy efficacy has an upward trend with augmenting Re and nano-additive concentration, and a decreasing trend with augmenting twisted ratio. At $\phi = 3\%$, by amplifying the Re from 7000 to 28000, the amount of exergy efficacy increases by 23.26%, 23.13%, 23.07 and 22.90% for cases of TIGs with $PR = 1$, 2, 3 and 4, respectively.

In general, with increasing Reynolds number, the Nu_{ave} which is an indicator of heat transfer rate, increases. On the other hand, also increment the volume fraction increases the heat conduction coefficient

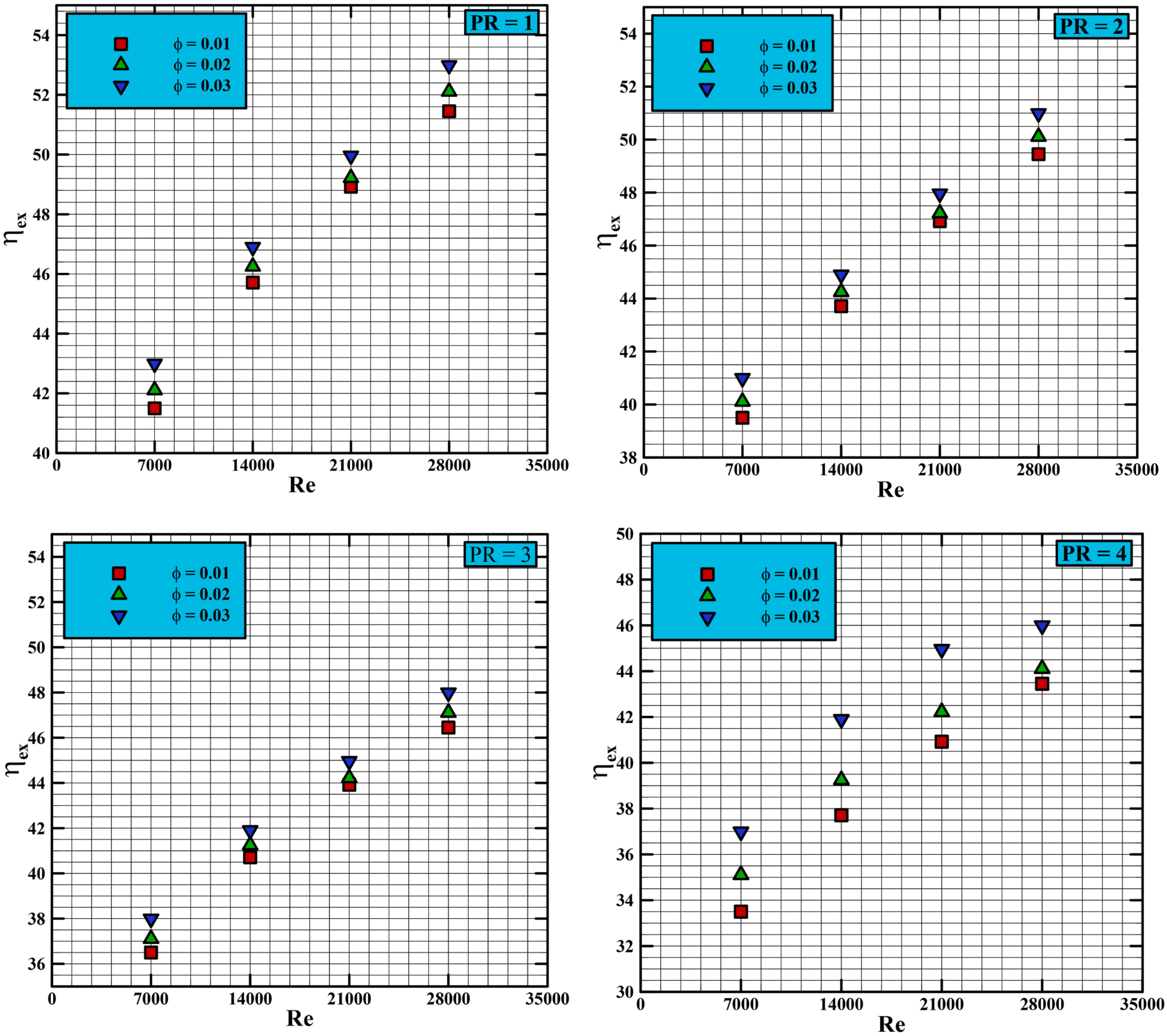

Fig. 12. Exergy efficacy versus Re in a SC containing a TIG with different twisted ratios and volume fractions.

and grows up the heat exchange. As a result, the efficiency of exergy increases. Also, enhancement of PR value increases the pressure drop and thus reduces the performance. As a result of reducing performance ability, the exergy efficiency decreases [33].

Conclusions

In this study, a special type of TIG with new geometries has been used. This TIG has been studied in several of PR values. The influence of TPHNF and TIGs on thermal–hydraulic performance, as well as exergy and energy efficacy of a SC in turbulent flow regime was investigated. A numerical study was performed for DWCNTs-TiO_2/water HNF with $1 \leq \phi \leq 3\%$, $7000 \leq Re \leq 28000$, and twisted ratios of 1, 2, 3, and 4. The results are as follows:

• At highest Re and ϕ, the installation of TIG with PR = 4 increases the Nu_{ave} and ΔP by 63.46% and 314.77%, respectively.

• The results revealed that the use of a novel TIG is desirable for the range of Re between 7000 and 28,000 and ϕ of 1% to 3%.

• Energy efficacy enhances by augmenting the twisted ratio of the TIG.

• In the case of $\phi = 3\%$ and by augmenting the Re from 7000 to 28000, energy and exergy efficacies increase by 22.19% and 23.26% for PR = 4 and PR = 1, respectively.

CRediT authorship contribution statement

Yacine Khetib: Formal analysis, Writing – original draft. **Ali Alzaed:** Writing – original draft. **Ahamd Tahmasebi:** Writing – review & editing. **Mohsen Sharifpur:** Conceptualization, Writing – review & editing. **Goshtasp Cheraghian:** Writing – review & editing.

Declaration of Competing Interest

The authors declare that they have no known competing financial interests or personal relationships that could have appeared to influence the work reported in this paper.

Acknowledgment

This work was supported by the Taif University Researchers

Supporting Project, Taif University, Taif, Saudi Arabia, under Project TURSP-2020/240.

References

[1] Ghalandari M, Maleki A, Haghighi A, Safdari Shadloo M, Alhuyi Nazari M, Tlili I. Applications of nanofluids containing carbon nanotubes in solar energy systems: a review. J Mol Liq 2020;313:113476.
[2] He W, Namar MM, Li Z, Maleki A, Tlili I, Safdari Shadloo M. Thermodynamic analysis of a solar-driven high-temperature steam electrolyzer for clean hydrogen production. Appl Therm Eng 2020;172:115152.
[3] Rostami S, Sepehrirad M, Dezfulizadeh A, Hussein AK, Shahsavar Goldanlou A, Shadloo MS. Exergy optimization of a solar collector in flat plate shape equipped with elliptical pipes filled with turbulent nanofluid flow: a study for thermal management. Water 2020;12:2294.
[4] Attia MEH, Karthick A, Manokar AM, Driss Z, Kabeel AE, Sathyamurthy R, et al. Sustainable potable water production from conventional solar still during the winter season at Algerian dry areas: energy and exergy analysis. J Therm Anal Calorim 2020.
[5] Ahmadi MH, Ghazvini M, Sadeghzadeh M, Alhuyi Nazari M, Kumar R, Naeimi A, et al. Solar power technology for electricity generation: a critical review. Energy Sci Eng 2018;6:340–61.
[6] Naseri A, Bidi M, Ahmadi MH, Saidur R. Exergy analysis of a hydrogen and water production process by a solar-driven transcritical CO2 power cycle with Stirling engine. J Cleaner Prod 2017;158:165–81.
[7] Bhattacharyya S, Pathak M, Sharifpur M, Chamoli S, Ewim DRE. Heat transfer and exergy analysis of solar air heater tube with helical corrugation and perforated circular disc inserts. J Therm Anal Calorim 2020.
[8] Parsa SM, Rahbar A, Koleini MH, Davoud Javadi Y, Afrand M, Rostami S, et al. First approach on nanofluid-based solar still in high altitude for water desalination and solar water disinfection (SODIS). Desalination 2020;491:114592.
[9] Parsa SM, Rahbar A, Koleini MH, Aberoumand S, Afrand M, Amidpour M. A renewable energy-driven thermoelectric-utilized solar still with external condenser loaded by silver/nanofluid for simultaneously water disinfection and desalination. Desalination 2020;480:114354.
[10] Ghorbani B, Mehrpooya M, Sadeghzadeh M. Developing a tri-generation system of power, heating, and freshwater (for an industrial town) by using solar flat plate collectors, multi-stage desalination unit, and Kalina power generation cycle. Energy Convers Manage 2018;165:113–26.
[11] Ahmadi MH, Sorouri Ghare Aghaj S, Nazeri A. Prediction of power in solar stirling heat engine by using neural network based on hybrid genetic algorithm and particle swarm optimization. Neural Comput Appl 2013;22:1141–50.
[12] Sadeghzadeh M, Ahmadi MH, Kahani M, Sakhaeinia H, Chaji H, Chen L. Smart modeling by using artificial intelligent techniques on thermal performance of flat-plate solar collector using nanofluid. Energy Sci Eng 2019;7:1649–58.
[13] Zhu D, Wang B, Ma H, Wang H. Evaluating the vulnerability of integrated electricity-heat-gas systems based on the high-dimensional random matrix theory. CSEE J Power Energy Syst 2019;6:878–89.
[14] Li X, Gui D, Zhao Z, Li X, Wu X, Hua Y, et al. Operation optimization of electrical-heating integrated energy system based on concentrating solar power plant hybridized with combined heat and power plant. J Cleaner Prod 2021;289:125712.
[15] Hu M, Wang Y, Yan Z, Zhao G, Zhao Y, Xia L, et al. Hierarchical dual-nanonet of polymer nanofibers and supramolecular nanofibrils for air filtration with high filtration efficiency, low air resistance and high moisture permeation. J Mater Chem A 2021.
[16] Thalib MM, Vimala M, Manokar AM, Sathyamurthy R, Sadeghzadeh M, Sharifpur M. Energy, exergy and economic investigation of passive and active inclined solar still: experimental study. J Therm Anal Calorim 2021.
[17] Ghoghaei MS, Mahmoudian A, Mohammadi O, Shafii MB, Jafari Mosleh H, Zandieh M, et al. A review on the applications of micro-/nano-encapsulated phase change material slurry in heat transfer and thermal storage systems. J Therm Anal Calorim 2021;145:245–68.
[18] Aghayari R, Maddah H, Pourkiaei SM, Ahmadi MH, Chen L, Ghazvini M. Theoretical and experimental studies of heat transfer in a double-pipe heat exchanger equipped with twisted tape and nanofluid. Eur Phys J Plus 2020;135:252.
[19] Gan T, Ming T, Fang W, Liu Y, Miao L, Ren K, et al. Heat transfer enhancement of a microchannel heat sink with the combination of impinging jets, dimples, and side outlets. J Therm Anal Calorim 2020;141:45–56.
[20] Eshgarf H, Kalbasi R, Maleki A, Shadloo MS, karimipour A. A review on the properties, preparation, models and stability of hybrid nanofluids to optimize energy consumption. J Therm Anal Calorim 2021;144:1959–83.
[21] Wang N, Maleki A, Alhuyi Nazari M, Tlili I, Safdari Shadloo M. Thermal conductivity modeling of nanofluids contain MgO particles by employing different approaches. Symmetry 2020;12:206.
[22] Baghban A, Sasanipour J, Pourfayaz F, Ahmadi MH, Kasaeian A, Chamkha AJ, et al. Towards experimental and modeling study of heat transfer performance of water- SiO2 nanofluid in quadrangular cross-section channels. Eng Applications Comput Fluid Mech 2019;13:453–69.
[23] Nasirzadehroshenin F, Sadeghzadeh M, Khadang A, Maddah H, Ahmadi MH, Sakhaeinia H, et al. Modeling of heat transfer performance of carbon nanotube nanofluid in a tube with fixed wall temperature by using ANN–GA. Eur Phys J Plus 2020;135:217.
[24] He J, Liu X, Song L, Li H, Zu H, Li J, et al. High annealing stability of InAlZnO nanofiber field-effect transistors with improved morphology by Al doping. J Phys Chem Lett 2021;12:1339–45.
[25] Tang Y, Cong H, Wang Z, Cheng H-M. Catalyst-seeded synthesis and field emission properties of flowerlike Si-doped AlN nanoneedle array. Appl Phys Lett 2006;89:253112.
[26] Xie Y, Meng X, Mao D, Qin Z, Wan L, Huang Y. Homogeneously dispersed graphene nanoplatelets as long-term corrosion inhibitors for aluminum matrix composites. ACS Appl Mater Interfaces 2021;13:32161–74.
[27] Ding H, Bao X, Jamili-Shirvan Z, Jin J, Deng L, Yao K, et al. Enhancing strength-ductility synergy in an ex situ Zr-based metallic glass composite via nanocrystal formation within high-entropy alloy particles. Mater Des 2021;210:110108.
[28] Afshari F, Sözen A, Khanlari A, Tuncer AD, Şirin C. Effect of turbulator modifications on the thermal performance of cost-effective alternative solar air heater. Renewable Energy 2020;158:297–310.
[29] Sakhaei SA, Valipour MS. Thermal performance analysis of a flat plate solar collector by utilizing helically corrugated risers: an experimental study. Sol Energy 2020;207:235–46.
[30] Hosseini SS, Farhadi M, Sedighi K. Experimental investigation of a solar desalination system using twisted tape and wire coil inside of spiral heat exchanger. Desalination 2017;420:34–44.
[31] Ibrahim M, Berrouk AS, Algehyne EA, Saeed T, Chu Y-M. Numerical evaluation of exergy efficiency of innovative turbulators in solar collector filled with hybrid nanofluid. J Therm Anal Calorim 2021:1–16.
[32] Yan S-R, Golzar A, Sharifpur M, Meyer JP, Liu D-H, Afrand M. Effect of U-shaped absorber tube on thermal-hydraulic performance and efficiency of two-fluid parabolic solar collector containing two-phase hybrid non-Newtonian nanofluids. Int J Mech Sci 2020;185:105832.
[33] Goldanlou AS, Sepehrirad M, Dezfulizadeh A, Golzar A, Badri M, Rostami S. Effects of using ferromagnetic hybrid nanofluid in an evacuated sweep-shape solar receiver. J Therm Anal Calorim 2021;143:1623–36.
[34] Waghole DR, Warkhedkar R, Shrivastva R. Experimental investigations on heat transfer and friction factor of silver nanofliud in absorber/receiver of parabolic trough collector with twisted tape inserts. Energy Procedia 2014;45:558–67.
[35] Nazir MS, Ghasemi A, Dezfulizadeh A, Abdalla AN. Numerical simulation of the performance of a novel parabolic solar receiver filled with nanofluid. J Therm Anal Calorim 2021;144:2653–64.
[36] Reddy K, Kumar KR, Ajay C. Experimental investigation of porous disc enhanced receiver for solar parabolic trough collector. Renewable Energy 2015;77:308–19.
[37] Ma Y, Jamiatia M, Aghaei A, Sepehrirad M, Dezfulizadeh A, Afrand M. Effect of differentially heated tubes on natural convection heat transfer in a space between two adiabatic horizontal concentric cylinders using nano-fluid. Int J Mech Sci 2019;163:105148.
[38] Reddy K, Kumar KR, Satyanarayana G. Numerical investigation of energy-efficient receiver for solar parabolic trough concentrator. Heat Transfer Eng 2008;29:961–72.
[39] Jaramillo O, Borunda M, Velazquez-Lucho K, Robles M. Parabolic trough solar collector for low enthalpy processes: An analysis of the efficiency enhancement by using twisted tape inserts. Renewable Energy 2016;93:125–41.
[40] Zhu X, Zhu L, Zhao J. Wavy-tape insert designed for managing highly concentrated solar energy on absorber tube of parabolic trough receiver. Energy 2017;141:1146–55.
[41] Dezfulizadeh A, Aghaei A, Joshaghani AH, Najafizadeh MM. Exergy efficiency of a novel heat exchanger under MHD effects filled with water-based Cu–SiO 2-MWCNT ternary hybrid nanofluid based on empirical data. J Therm Anal Calorim 2021:1–24.
[42] Abdollahzadeh M, Sedighi AA, Esmailpour M. Stagnation point flow of nanofluids towards stretching sheet through a porous medium with heat generation. J Nanofluids 2018;7:149–55.
[43] Rahimi A, Kasaeipoor A, Malekshah EH, Kolsi L. Experimental and numerical study on heat transfer performance of three-dimensional natural convection in an enclosure filled with DWCNTs-water nanofluid. Powder Technol 2017;322:340–52.
[44] Sadripour S, Chamkha AJ. The effect of nanoparticle morphology on heat transfer and entropy generation of supported nanofluids in a heat sink solar collector. Thermal Sci Eng Progress 2019;9:266–80.
[45] I. Ansys, Cfx-solver theory guide, Release 12.1 ed., (2009).
[46] Behzadmehr A, Saffar-Avval M, Galanis N. Prediction of turbulent forced convection of a nanofluid in a tube with uniform heat flux using a two phase approach. Int J Heat Fluid Flow 2007;28:211–9.
[47] Hejazian M, Moraveji MK, Beheshti A. Comparative study of Euler and mixture models for turbulent flow of Al2O3 nanofluid inside a horizontal tube. Int Commun Heat Mass Transfer 2014;52:152–8.
[48] Göktepe S, Atalık K, Ertürk H. Comparison of single and two-phase models for nanofluid convection at the entrance of a uniformly heated tube. Int J Therm Sci 2014;80:83–92.
[49] Afrand M, Farahat S, Nezhad AH, Ali Sheikhzadeh G, Sarhaddi F. 3-D numerical investigation of natural convection in a tilted cylindrical annulus containing molten potassium and controlling it using various magnetic fields. Int J Appl Electromagnet Mech 2014;46:809–21.
[50] Afrand M. Using a magnetic field to reduce natural convection in a vertical cylindrical annulus. Int J Therm Sci 2017;118:12–23.
[51] Li Z, Du C, Ahmadi D, Kalbasi R, Rostami S. Numerical modeling of a hybrid PCM-based wall for energy usage reduction in the warmest and coldest months. J Therm Anal Calorim 2021;144:1985–98.
[52] Afrand M, Farahat S, Nezhad AH, Sheikhzadeh GA, Sarhaddi F, Wongwises S. Multi-objective optimization of natural convection in a cylindrical annulus mold

under magnetic field using particle swarm algorithm. Int Commun Heat Mass Transfer 2015;60:13–20.
[53] Afrand M, Farahat S, Nezhad AH, Sheikhzadeh GA, Sarhaddi F, Numerical simulation of electrically conducting fluid flow and free convective heat transfer in an annulus on applying a magnetic field, 45 (2014) 749-766.
[54] Sheikholeslami M, Gorji-Bandpy M, Ganji D. Effect of discontinuous helical turbulators on heat transfer characteristics of double pipe water to air heat exchanger. Energy Convers Manage 2016;118:75–87.